RSC Advances

PAPER

View Article Online
View Journal | View Issue

Check for updates

Cite this: *RSC Adv.*, 2020, **10**, 16490

Open Access Article. Published on 25 April 2020. Downloaded on 2/25/2026 9:47:25 AM.
This article is licensed under a Creative Commons Attribution-NonCommercial 3.0 Unported Licence.

A multiple model approach for evaluating the performance of time-lapse capsules in trapping heavy metals from water bodies†

Shu-Yuan Pan, * Wei-Jhan Syu, Tsun-Kuo Chang and Cheng-Hsun Lee

Received 3rd April 2020
Accepted 7th April 2020

DOI: 10.1039/d0ra03017a

rsc.li/rsc-advances

Adsorption by ion-exchange resins has been widely used as a cost-effective method for removing numerous hazardous materials, particularly heavy metals, from aqueous solutions. For effectively detecting the illegal discharge of industrial wastewater containing heavy metals, we developed "time-lapse capsules" to trap metallic ions from water bodies. Despite recent progress in the development of time-lapse capsules, a fundamental understanding was still needed to unravel the adsorption behavior of different heavy metals for further improvement of the design and scale-up of the capsule. In this study, three different approaches, *viz.*, response surfaces (from the statistical point of view), time-dependent diffusion-controlled models (from the kinetic point of view), and adsorption isotherms (from the equilibrium point of view), were utilized to evaluate the effect of operating factors on the adsorption of heavy metals from watershed using time-lapse capsules. The obtained results indicated that the key parameters, such as adsorption rate constant, diffusivity, and maximum adsorption capacity, could provide insights into the basis of design criteria.

1. Introduction

A water body is generally defined as a body of accumulated water forming a physiographical feature on a planet's surface, such as oceans, watersheds, lakes, wetlands, and reservoirs (even phytotelma). Illegal discharges of industrial wastewater containing heavy metals into water bodies, particularly rivers and streams, have been a critical issue in sustainable watershed management and source water protection around the world.[1,2] A polluted water body deteriorates the quality of irrigation water and thus, causes risk to the safety of crops and foods. Events of illegal discharges (wastewater) from industries, however, are usually intentional at a random time. In other words, this type of water pollution is difficult to identify because the sources of illegal discharges are hard to find out. On the other hand, the conventional analysis of heavy metals in water samples is relatively time-consuming and expensive, which makes the monitoring of heavy metal pollution in rivers unpractical. Therefore, the development of rapid and effective approaches for monitoring, sampling, and analysis of heavy metal pollution in water bodies are necessary.

For detecting illegal discharges of wastewater, Huang *et al.*[3] developed ion-exchange resin sachets (referred to as "time-lapse capsules" in this work) to trap metallic ions from the watershed, such as irrigation and drainage channels, throughout a certain period of time (usually >seven days). The time-lapse capsules were manufactured by packing a certain amount of ion-exchange resins into a non-woven fabric sachet. The time-lapse capsules were surrounded by a cylindrical polyethylene mesh to increase the mechanical durability. It is noted that the adsorption by ion-exchange resins has been used for various applications, such as removal of heavy metals,[4,5] removal of perfluoroalkyl substances,[6] removal of metal complexed azo dyes,[7] nutrient recovery from urine,[8] and precious metal recovery from electrical and electronic wastes.[9,10] The developed time-lapse capsules could be readily deployed in monitoring works and could serve as concentrators of heavy metals from a water body. Therefore, once there is an illegal discharge of wastewater at any time, the deployed time-lapse capsules in the watershed could trap the heavy metals from the wastewater. The concentration of the adsorbed heavy metals on the time-lapse capsules could also be rapidly determined by the non-destructive X-ray fluorescence core-scanning (XRF-CS) technique.[3,11] According to the results reported by Huang *et al.*,[3] the concentrations of heavy metals determined by the XRF-CS (the increase on the resin) and the conventional analytical method (the reduction in water) exhibited excellent correlations (R^2 > 0.97) even at a short scanning time (<1 s). By doing so, one could identify the potential hot spots of illegal discharge *in situ* and then keep deploying more time-lapse capsules upstream until the discharge point of the industry is located.

The efficiency of time-lapse capsules for the adsorption of metals from water bodies can be attributed to a number of

Department of Bioenvironmental Systems Engineering, National Taiwan University, Taipei City, 10617 Taiwan, Republic of China. E-mail: sypan@ntu.edu.tw

† Electronic supplementary information (ESI) available. See DOI: 10.1039/d0ra03017a

This journal is © The Royal Society of Chemistry 2020

Open Access Article. Published on 25 April 2020. Downloaded on 2/25/2026 9:47:25 AM. This article is licensed under a Creative Commons Attribution-NonCommercial 3.0 Unported Licence.

factors, such as the water flow rate in the channels, the chemistry between the metallic ions and the adsorbent, and the physico-chemical properties of ion exchange resins. From the theoretical point of view, the removal kinetics and equilibrium isotherms are essential for the effective design of the adsorption system. In general, the kinetics of adsorption by ion-exchange resins are governed by the extent of agitation, the initial concentration of the ions in the solution, the ionic size and mobility, the type of counter ions, and the nature of exchangers. The analysis of adsorption kinetics can provide information about the adsorption mechanism of heavy metals and the time required to reach equilibrium. Likewise, the adsorption isotherms can elucidate the interactions of the metal ions with the resins and estimate the adsorption capacity.[12,13] Extensive studies have been reported on the application of various ion-exchange resins for the removal of heavy metals from aqueous solutions. However, to the best of our knowledge, scarcely any study has been focused on the fundamental research of adsorption of heavy metals, such as kinetics and isotherms, especially using time-lapse capsules.

Despite recent progress in the development of time-lapse capsules, a fundamental understanding is still needed to unravel the adsorption behaviors of different heavy metals for further improvement of the design and scale-up of the capsules. In this study, multiple model approaches were utilized to evaluate the effect of the operating factors on the heavy metal trapping performance from water using time-lapse capsules. By using the experimental data, the response surfaces of key operating parameters (including initial concentration, stirring speed, and adsorption time) with respect to the performance of adsorption were established from the statistical point of view. Apart from this, the kinetics of adsorption of different metal ions were evaluated using classical heterogeneous models, such as pseudo-first-order, pseudo-second-order, and diffusion-controlled models. The adsorption isotherms (from the equilibrium point of view) were also determined at the equilibrium of the heterogeneous system. Therefore, by doing so, we could systematically understand the adsorption behaviors of different heavy metals using time-lapse capsules from different angles, which would be beneficial for the scale-up of operation and the improvement of design in the future.

2. Materials and methods

2.1 Materials

In this study, a sodium-type cation exchange resin (Amberlite™ IR120) was used to prepare the time-lapse capsule. Table S1 (see ESI†) presents the physico-chemical characteristics of the IR120 resin. The matrix of the resin was the styrene divinylbenzene copolymer with a sulfonate-based functional group, possessing a total exchange capacity of 2.00 eq L^{-1}. The detailed procedure for the preparation of time-lapse capsules can be found in our previous studies.[3,11]

2.2 Batch adsorption experiments

The adsorption of different metal ions (*i.e.*, Zn, Cu, Cr, Pb, Ni, Ca, Mn, and Ti) by the time-lapse capsules was evaluated in a batch system. For each metal ion, four different levels of concentrations (see Table S2†) were prepared in accordance with the Effluent Standards in Taiwan.[14] In order to study the effect of mixing, the adsorption experiments were performed using the Jar-Tester machine (JT-6, Shin-Kwang Precision Industry Ltd., Taiwan) at different stirring speeds, *i.e.*, 50, 100, 150, and 200 rpm at 20 °C for 2 h. The type of stirrer used in the Jar-Tester machine was a single straight blade with a length of 8 cm and a width of 2 cm (SAE 304 stainless steel). The volume of solution for each batch test was one liter and 20 g of the ion exchange resin was used in each time-lapse capsule. After the experiment was finished, the time-lapse capsule was removed from the solution and the residual amounts of metal ions in the solution were analyzed by ICP-OES (Agilent 5110, USA).

The removal efficiency of the metal ions (R) was calculated using eqn (1):

$$R_i\,(\%) = \frac{C_o - C_e}{C_o} \times 100 \tag{1}$$

where C_o and C_e are the initial and equilibrium concentration (mg L^{-1}) of metal i in the solution, respectively. In this study, the effect of different operating parameters, including initial concentration (four levels for each metal, see Table S2†), stirring speed (50, 100, 150, and 200 rpm), and adsorption time (0, 0.5, 1, 3, 5, 10, 20, 30, 60, and 120 min), on the removal efficiency of metals was evaluated. The Design Expert software (StatEase Inc., Minneapolis, USA) was used to develop non-linear regression programs.

The amount of metal ion adsorbed onto a unit dry mass of the resin (q_e) can be determined by mass balance using eqn (2):

$$q_e\left(\text{mg g}^{-1}\right) = \frac{C_o - C_e}{m} \times V \tag{2}$$

where V is the volume of the solution (L) in each batch experiment and m is the mass of the ion exchange resin (g).

2.3 Kinetic adsorption models

The contact time between the adsorbate and the adsorbent is an important factor as ion removal through adsorption could occur on the solid–liquid interface. Adsorption kinetics can provide information regarding the rate of removal of ions using the time-lapse capsules as well as the controlling mechanisms of adsorption processes such as chemical reactions and/or mass transfer. The kinetic parameters play a vital role in the design and scale-up of the adsorption process. In order to evaluate the reaction kinetics of ion (adsorbate) removal using the time-lapse capsules, different types of models, including pseudo-first-order, pseudo-second-order, and diffusion-controlled mechanism, were applied in this study.

2.3.1 Pseudo-first-order kinetics. The pseudo-first-order kinetic model, so-called the Lagergren equation,[15] was used to describe a sorption system with the liquid and solid interface based on the solid capacity. The linearized form of the pseudo-first-order rate equation can be expressed as follows:

$$\log(q_e - q_t) = \log q_e - \frac{k_1}{2.303}t \tag{3}$$

Open Access Article. Published on 25 April 2020. Downloaded on 2/25/2026 9:47:25 AM. This article is licensed under a Creative Commons Attribution-NonCommercial 3.0 Unported Licence.

$$\log\left(1-\frac{q_t}{q_e}\right) = -\frac{k_1}{2.303}t \tag{4}$$

where q_t (mg g^{-1}) is the amount of metal ion adsorbed at time t (min) and k_1 (min^{-1}) represents the pseudo-first-order rate constant.

2.3.2 Pseudo-second-order kinetics. In the pseudo-second-order model developed by Ho *et al.*,[16] it was assumed that the rate limiting step of the process should be related to the valence forces due to electron sharing between the functional groups and metal ions. The linearized form of the rate equation can be expressed as follows:

$$\frac{t}{q_t} = \frac{1}{{q_e}^2} \times \frac{1}{k_2} + \frac{t}{q_e} \tag{5}$$

where k_2 (g mg^{-1} min^{-1}) indicates the pseudo-second-order rate constant.

2.3.3 Diffusion-controlled kinetics. During the adsorption process, typically, there are four different stages, *viz.*, (i) bulk diffusion: from the bulk solution to the outer surface of the liquid film, (ii) external diffusion: from the liquid film to the surface of the solid adsorbent, (iii) intraparticle diffusion: from the surface of the adsorbent to the intraparticular sites, and (iv) adsorption on the interior of the porous adsorbent. In general, with sufficient agitation, bulk diffusion limit can be neglected as particle and solute gradients in the batch reactor are avoided. Therefore, intraparticle diffusion and external diffusion are usually considered as the rate controlling steps of an adsorption process.

If external diffusion of metal ions (within the diffuse layers outside the sorbent) is the rate limiting factor, the adsorption data can be described by eqn (6):

$$\ln(C_t/C_o) = -k_f(A/V) \times t \tag{6}$$

where C_t is the concentration (mg L^{-1}) of metal i in the solution at time t (min), k_f is the external diffusion coefficient, and A/V is the ratio of external sorption area to the volume of the total solution (m^{-1}). Ion exchange resins with an A/V value of 428 m^{-1} were reported in the literature.[17]

If the intraparticle diffusion model is the rate limiting step, the experimental data could be described by the following model:[18]

$$q_t = k_p t^{1/2} + I \tag{7}$$

where k_p (mg g^{-1} min$^{-1/2}$) denotes the intraparticle diffusion rate constant and I is the intercept reflecting the effect (thickness) of the boundary layer (mg g^{-1}).

2.4 Adsorption isotherms

The adsorption isotherms can provide insights on the equilibrium between the metal ions presented in the solution and on the adsorbent at a certain temperature. The extent of the adsorption capacity depends on several factors, such as the theoretical capacity of the ion exchange resin, the selectivity of the adsorbent over other ions present in the solution, and the approximation rate to the equilibrium load. In this study, the Langmuir, Freundlich, Temkin, and Dubinin–Radushkevich isotherm models were used to describe the equilibrium data and to evaluate the surface properties of the adsorbent and its adsorption behaviors.

2.4.1 Langmuir isotherm. The Langmuir model was used based on the assumption of surface homogeneity, such as equally available adsorption sites and monolayer surface coverage. It was assumed that there was no interaction between the adsorbed species. It was noted that this model would be applicable to the adsorption of inorganic and/or organic pollutants from aqueous solutions. The linearized form of the Langmuir model can be expressed as follows:

$$\frac{C_e}{q_e} = \frac{C_e}{q_m} + \frac{1}{K_L q_m} \tag{8}$$

where q_m (mg g^{-1}) indicates the maximum adsorption capacity of the adsorbent and K_L (L mg^{-1}) is the Langmuir constant related to the energy of adsorption.

2.4.2 Freundlich isotherm. The Freundlich model is applicable to the heterogeneous system and reversible adsorption. The linearized form of the Freundlich model can be described as follows:

$$\ln(q_e) = \ln(K_F) + \frac{1}{n}\ln(C_e) \tag{9}$$

where K_F is the Freundlich constant representing the strength of the adsorptive bond and n is the Freundlich exponent, known as the adsorbent intensity of the adsorbent, indicating the favorability of the adsorption process. The value of $1/n$ is a measure of the surface heterogeneity, which ranges between 0 and 1, and becomes more heterogeneous when approached to zero.[7] It also represents the distribution of site energies: the value of $n - 1$ ranging between 0.1 and 0.5 indicated that the adsorption should be favorable; the value of $n - 1$ ranging between 0.5 and 1.0 represented that the ions are easy to adsorb; otherwise (if $n - 1 > 1$), it is difficult to adsorb.

2.4.3 Temkin isotherm. The Temkin model was developed based on the assumption that the free energy of adsorption is a function of the surface coverage. The linearized form of the Temkin model is represented in eqn (10):

$$q_e = \frac{RT}{b} \times \ln(K_T) + \frac{RT}{b} \times \ln(C_e) \tag{10}$$

where K_T (L g^{-1}) is the Temkin constant, representing the equilibrium binding constant related to the maximum binding energy, b (J mol^{-1}) is a constant related to the heat of adsorption, R (8.314 J K^{-1} mol^{-1}) is the universal gas constant, and T (K) is the absolute temperature.

2.4.4 Dubinin–Radushkevich (D–R) isotherm. To elucidate the adsorption mechanism (*i.e.*, physisorption or chemisorption), the experimental data were applied to the Dubinin–Radushkevich (D–R) model. This model was developed based on the adsorption mechanism with a Gaussian energy distribution on a heterogeneous surface. The linearized form of the D–R model is provided as follows:

$$\ln(q_e) = \ln(q_m) - \beta\varepsilon^2 \tag{11}$$

 This journal is © The Royal Society of Chemistry 2020

Open Access Article. Published on 25 April 2020. Downloaded on 2/25/2026 9:47:25 AM.
This article is licensed under a Creative Commons Attribution-NonCommercial 3.0 Unported Licence.

where β (mol^2 kJ^{-2}) is the D–R constant related to sorption energy. ε (kJ mol^{-1}) is the Polanyi potential, which is mathematically represented as:

$$\varepsilon = RT\ln(1 + 1/C_e) \tag{12}$$

By assuming that the adsorbate was transferred from infinity in the solution to the surface of the resin,[19] the mean free energy of adsorption per molecule of the adsorbate (E, kJ mol^{-1}) can be determined by eqn (13).

$$E = \frac{1}{\sqrt{2\beta}} \tag{13}$$

This parameter can provide information about the mechanism of adsorption:[20–22] (i) the adsorption process was followed by ion-exchange if E was between 8–16 kJ mol^{-1}, or (ii) by physical adsorption if E was less than 8 kJ mol^{-1}. It was noted that E value less than 8 kJ mol^{-1} indicated a weak sorbent–sorbate interaction, which might lead to subsequent release of the adsorbed metal ions back into the solution from the surface of the adsorbent after sorption equilibrium.

3. Results and discussion

3.1 Effect of initial concentration, stirring speed, and adsorption time on metal trapping

In this study, the performance of time-lapse capsules for heavy metal adsorption from water bodies was evaluated by using the batch adsorption experiments. The variable parameters include initial concentration (four levels for each metal, see Table S2†), stirring speed (50, 100, 150, and 200 rpm), and adsorption time (0, 0.5, 1, 3, 5, 10, 20, 30, 60, and 120 min), thereby resulting in a total of 144 experimental data for each metal. Fig. 1 shows the effect of different adsorption (contact) times and initial concentrations on the removal of metal ions in terms of the amounts of metal ions adsorbed on the resins (q_t, mg g^{-1}) at a stirring speed of 200 rpm. We found that the adsorption of metal ions on the resins could proceed *via* two stages in the period of contact as follows: (i) rapid uptake and (ii) slow adsorption. For the first stage, the value of q_t increased rapidly as the adsorption (contact) time increased from 0 to 40 min, especially within the first 20 min. After 40 min, the value of q_t became relatively constant (the second stage), indicating that equilibrium was reached. The phenomena of this two-stage adsorption might be attributed to the available active sites on the ion-exchange resins. Rapid uptake of metal ions occurred due to a great number of active sites on the surface of the resins that were readily accessible at the beginning of the adsorption experiments. The rate of adsorption decreased thereafter as the active sites on the resins were gradually occupied by metal ions.

Similarly, with the increase in the initial concentrations of the metal ions, the value of q_t increased accordingly. Different initial concentrations would thus correspond to different levels of the final equilibrium saturation adsorption capacity (q_e). Aside from the active sites on the resins, for the first stage, the slope of the adsorption curve (*i.e.*, Zn, Cu, Cr, Ni, Ca, and Mn) at higher initial concentration was steeper due to the higher concentration gradient. The higher concentration gradient could provide a greater driving force to overcome resistance to external mass transfer (*i.e.*, film diffusion) between the solution and the resin phases. It is noteworthy that the adsorption kinetics and capacities could be affected by the design of the time-lapse capsules, such as the particle size and packing density of the resins. The adsorption kinetics generally increased as the particle size of the resins decreased. For adsorption capacities, the packing density of the resins in a time-lapse capsule should be determined based on the expected concentrations of heavy metals in water bodies to avoid over-saturated adsorption.

Based on these experimental data, we formulated non-linear programs to evaluate the effect of the initial concentration, stirring speed, and adsorption time on the efficiency of

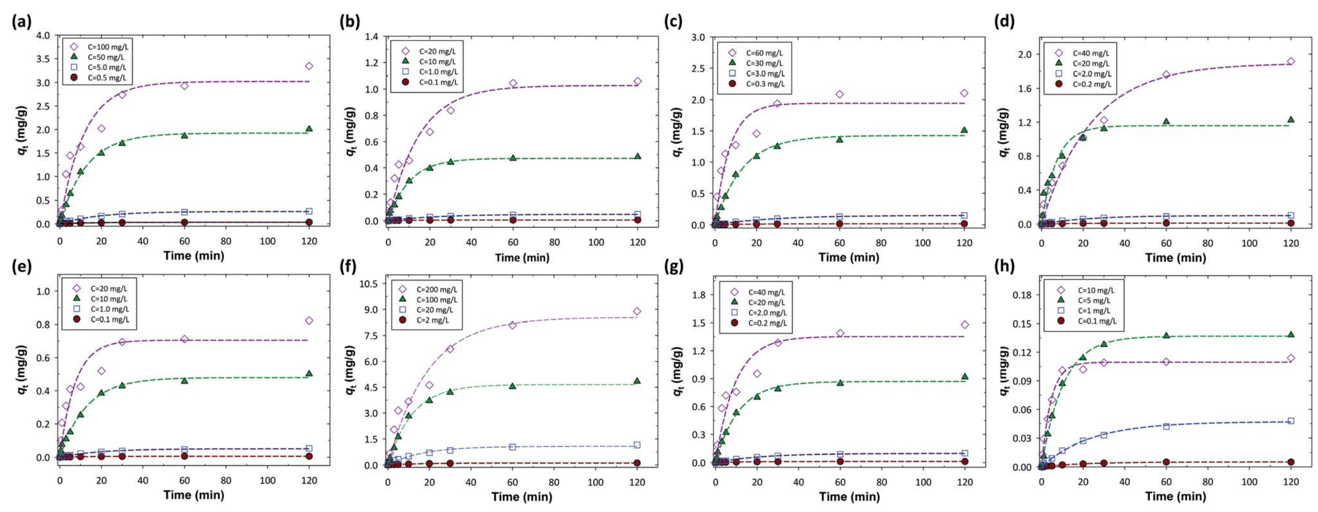

Fig. 1 Effect of different adsorption times and initial concentrations on the removal of (a) Zn, (b) Cu, (c) Cr, (d) Pb, (e) Ni, (f) Ca, (g) Mn, and (h) Ti using time-lapse capsules at a stirring speed of 200 rpm.

Open Access Article. Published on 25 April 2020. Downloaded on 2/25/2026 9:47:25 AM.
This article is licensed under a Creative Commons Attribution-NonCommercial 3.0 Unported Licence.

Table 1 Models of removal efficiency for different metal ions in terms of coded operating factors according to the experimental data ($n = 144$ for each equation)

Metal	Response surface model (in terms of removal efficiency)[a]	Eqn.	R^2
Zn	$Zn = 0.54 + 0.24A + 0.29B - 0.10C + 0.16AB - 0.08AC - 0.07BC - 0.27A^2$	(14)	0.864
Cu	$Cu = 0.46 + 0.18A + 0.31B - 0.28C + 0.18AB - 0.14AC - 0.25A^2 - 0.17C^2$	(15)	0.848
Cr	$Cr = 0.58 + 0.29A + 0.40B - 0.28C + 0.19AB - 0.27A^2 - 0.11B^2 - 0.23C^2$	(16)	0.876
Pb	$Pb = 0.51 + 0.17A + 0.27B - 0.15C + 0.18AB - 0.12AC - 0.16BC - 0.29A^2 - 0.11B^2$	(17)	0.862
Ni	$Ni = -0.38 - 0.08A + 0.07B - 2.11C + 0.16AB - 0.39AC - 0.30BC - 0.23A^2 - 0.07B^2 - 1.11C^2$	(18)	0.869
Ca	$Ca = 0.63 + 0.29A + 0.40B - 0.03C + 0.19AB - 0.03AC - 0.03BC - 0.27A^2 - 0.10B^2$	(19)	0.872
Mn	$Mn = 0.43 + 0.11A + 0.38B - 0.23C + 0.17AB - 0.21AC - 0.26A^2 - 0.12B^2$	(20)	0.856
Ti	$Ti = -0.30 - 0.49A - 0.13B - 0.91C + 0.13AB - 0.82AC - 0.47BC - 0.22A^2 - 0.08B^2$	(21)	0.857

[a] A, B, and C are coded and denoted as the adsorption time (min), stirring speed (rpm), and concentration in water (mg L^{-1}), respectively.

adsorption of the metals. Table 1 presents the results of non-linear programs for describing the adsorption behaviors of metals in terms of different operating parameters. Based on the experimental data, the non-linear programs were developed to predict the response of system performance from the statistical point of view. In the non-linear programs, A, B, and C were coded parameters and denoted as the adsorption time (min), stirring speed (rpm), and concentration in water (mg L^{-1}), respectively. For the adsorption behavior of all the metals, we found that the modified quadratic programs were the best fitting models as the p-value of all the models was less than 0.0001 (CI: 95%). The coefficients of determination (R^2) for all the developed models were in the range between 0.848 and 0.876. The analysis of variance (ANOVA) results of the developed models for different metals are summarized in the ESI (Tables S1–S8†), indicating that the adsorption of metals, especially Zn, Cu, Cr, Ca, and Mn, could be well described by the developed models. Based on these developed models, we could easily visualize the performance of metal trapping under different operating conditions, identify the effect of operating parameters on the removal efficiency, and determine the maximum efficiency at certain constraint conditions.

Fig. 2 shows the response surfaces of the developed models for the removal (adsorption) efficiency of different metals, in terms of adsorption time and stirring speed. The results indicated that for all the metals, the removal efficiency increased as both the adsorption time and stirring speed increased. According to the coefficients of each term in the equations (Table 1), the stirring speed (denoted as B) exhibited the most positive influence on the removal efficiency. In other words, compared to the adjustment of other parameters, it was more effective to enhance the removal efficiency by increasing the stirring speed from 50 to 200 rpm. The sequence of metal removal efficiency on increasing one unit of stirring speed was in the order: Cr ∼ Ca > Mn > Cu > Zn > Pb > Ni > Ti. The extent of mixing (stirring) could be attributed to the rate of the diffusion-controlled step for surface sorption from the liquid phase onto the surface of the solid resin. It was noted that the mass transfer considerations for adsorption included (i) convection and diffusion through the liquid film surrounding the resin (so-called film diffusion), (ii) diffusion along the length of a pore (so-called pore diffusion), and (iii) adsorption onto the vacant site of the solid surface.[23] Sufficient mixing between the water samples and the time-lapse capsules could effectively promote

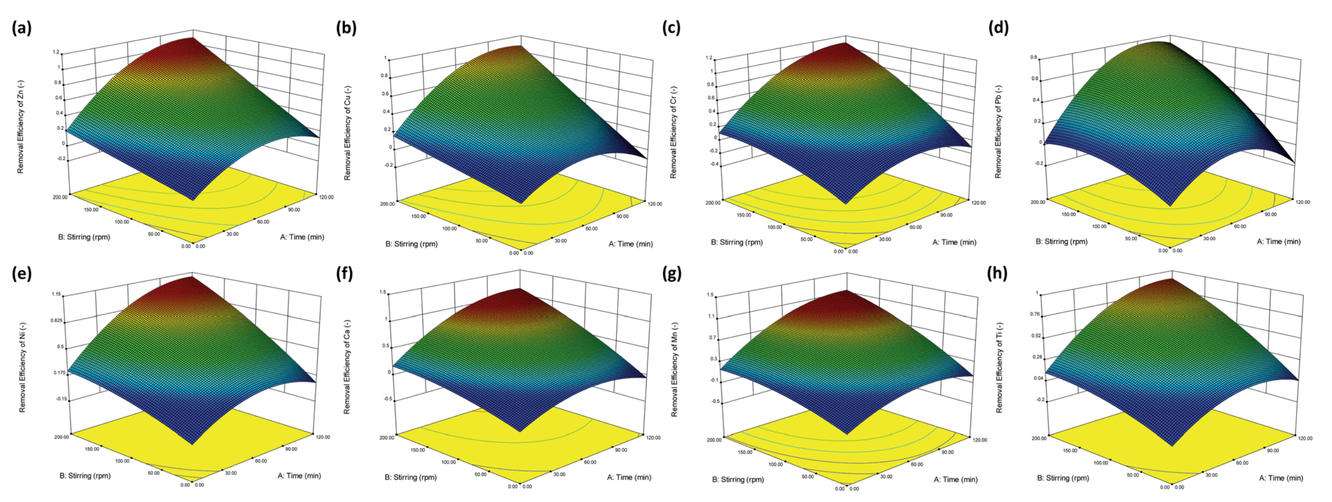

Fig. 2 Effect of adsorption time and stirring speed on the removal efficiency of (a) Zn, (b) Cu, (c) Cr, (d) Pb, (e) Ni, (f) Ca, (g) Mn, and (h) Ti ions in water. The initial concentrations of each metal: Zn (25 mg L^{-1}), Cu (50 mg L^{-1}), Cr (50 mg L^{-1}), Pb (5 mg L^{-1}), Ni (5 mg L^{-1}), Ca (50 mg L^{-1}), Mn (0.5 mg L^{-1}), and Ti (5 mg L^{-1}). Other operating factors: adsorption at 20 °C using 20 g of ion exchange resin in a time-lapse capsule.

This journal is © The Royal Society of Chemistry 2020

Open Access Article. Published on 25 April 2020. Downloaded on 2/25/2026 9:47:25 AM.
This article is licensed under a Creative Commons Attribution-NonCommercial 3.0 Unported Licence.

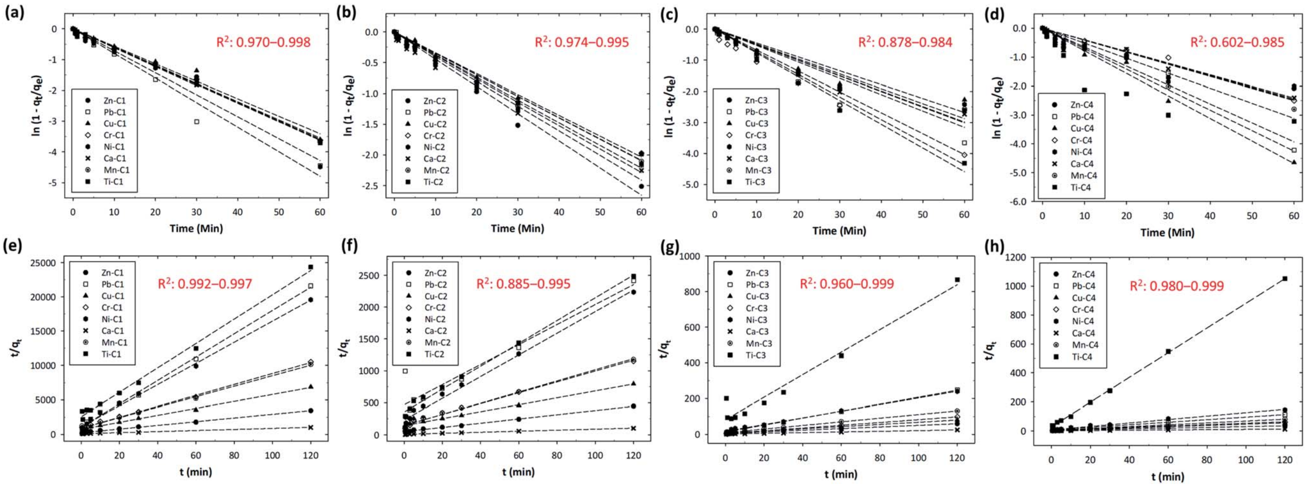

Fig. 3 Pseudo-first-order kinetic curves (Lagergren plot) for specific rate constant of metal ions on time-lapse capsules at different initial concentrations: (a) C1, (b) C2, (c) C3, and (d) C4. Pseudo-second-order kinetic curves at different initial concentrations: (e) C1, (f) C2, (g) C3, and (h) C4.

the rate of film diffusion, thereby shortening the time required to reach equilibrium. Thus, in the following analyses, including kinetics and adsorption isotherm, the stirring speed was fixed at 200 rpm to ensure rapid mass transfer in the bulk solution.

The removal efficiency of the metals could also be enhanced by prolonging the adsorption time, especially for the first 40 min. According to the coefficient of term *A* in the equations (Table 1), a similar trend of metal removal efficiency on increasing one unit of adsorption time was noticed: Cr ∼ Ca > Zn > Cu ∼ Pb > Mn > Ni > Ti. However, once the maximum adsorption capacity of the resins (the saturation point, or sometimes called as the equilibrium distribution) was reached, the removal efficiency remained almost unchanged, even when the adsorption time was further prolonged. It was noted that the adsorption of metals could be considered as a partitioning of the adsorbate (ions) between the liquid phase and the resin adsorbent.[23] In the following analyses, we studied several adsorption isotherm and kinetic models to elucidate the equilibrium behaviors and adsorption rates.

3.2 Adsorption kinetics

Among the operating factors (adsorption time, stirring speed, and concentration) used in this study, the stirring speed was the most dominant factor affecting the adsorption efficiency of all the metals. In a real watershed, the water flow rate is usually high enough to ensure complete mixing, *i.e.*, the concentration difference of the metals within the liquid film surrounding the resin might not be significant. Therefore, to evaluate the adsorption kinetics of different metals using time-lapse capsules, we neglected the limiting step of film diffusion by analyzing the experimental data with the highest designated stirring speed (*i.e.*, 200 rpm). In this study, the adsorption kinetic models were established using two different approaches based on (i) the adsorption capacity of the solid adsorbent and (ii) the type of diffusion-controlled mechanism.

3.2.1 Sorption rate constant and capacity. For kinetics based on the adsorption capacity of the solid adsorbent, we applied the pseudo-first-order (eqn (4)) and pseudo-second-order (eqn (5)) models on the experimental data. Fig. 3 shows the fitting curves at different initial concentrations accompanied by the least-squares regression analysis of the models. Comparing the coefficients of determination, it was found that the pseudo-second-order model was well fitted to the experimental data in all the cases with very high precision. This indicated that the adsorption of heavy metals using time-lapse capsules was controlled by adsorbate diffusion rather than surface control and chemisorption might be the dominant mechanism.[24] In the pseudo-second-order model, the rate of adsorption was related to the squared product of the difference between the occupied sites and the total number of equilibrium adsorption sites available on the adsorbent.[25] However, in the pseudo-first-order model, it was assumed that the rate of adsorption would be attributed to the number of unoccupied active sites on the surface of the resins. Therefore, the pseudo-first-order model could be employed to describe the first stage of rapid uptake (*e.g.*, before 30 min in this study). At the second stage of slow adsorption, resistance due to pore diffusion would change the rate of ion exchange to a non-linear relationship, where the second-order model could be applied.[26] At the concentration in accordance with Taiwan EPA's effluent standards (*i.e.*, C2), the obtained values of k_2 for Zn, Pb, Cu, Cr, Ni, Ca, Mn, and Ti were 0.21, 0.53, 0.20, 0.49, 1.25, 0.07, 0.52, and 0.90 g mg^{-1} min^{-1}, respectively.

Table 2 summarizes the kinetic data extracted from the pseudo-first and pseudo-second order models for the adsorption of metal ions using time-lapse capsules at 20 °C. Based on the obtained pseudo-second-order rate constant, the half-adsorption time ($t_{1/2}$) for different metals was determined. The half-adsorption time was defined as the time required to reach half the amount of the maximum adsorption capacity by the ion-exchange resins. The half-adsorption time could be used as a measure of the adsorption rate, as described by eqn (22).[27]

$$t_{1/2} = \frac{1}{k_2 q_e} \tag{22}$$

The results indicated that the half-adsorption time was not necessarily proportional to the initial concentration of the metals in the water bodies. In most cases, the half-adsorption time firstly increased as the initial concentration increased from C1 to C2 (*e.g.*, Zn, Pb, Ni, and Mn) or from C1 to C3 (*e.g.*, Cu), and then rapidly decreased if the initial concentration further increased to C4.

3.2.2 Film-pore diffusion mechanism. In general, the mechanism of adsorption of metals on ion-exchange resins may involve three steps: (i) diffusion of metals through the boundary layer, (ii) intraparticle diffusion, and (iii) adsorption of metals on the surface of the resins. According to the results from Fig. 3, it is understood that the rate of adsorption of metal ions would be mainly governed by adsorbate diffusion rather than surface control. As a result, we applied the film-pore diffusion models, *i.e.*, external diffusion (eqn (6)) and intraparticle diffusion (eqn (7)), to further identify the type of diffusion-controlled mechanism. Table 3 summarizes the kinetic data extracted from the film-pore diffusion models for the adsorption of metal ions using time-lapse capsules at 20 °C. The results indicated that the rate-limiting step of metal ion adsorption would be external diffusion control at low initial concentrations. The external diffusion coefficients of all the metal ions were not significantly different from each other, as the adsorption studies of all the experiments were conducted at the same temperature. It was noted that the mass diffusion coefficient would be largely dependent on the temperature of the solution, according to the Stokes–Einstein equation. For the concentration in accordance with Taiwan EPA's effluent standards (*i.e.*, C2), the obtained external diffusion coefficients (k_f) for Zn, Pb, Cu, Cr, Ni, Ca, Mn, and Ti were 0.10, 0.12, 0.11, 0.09, 0.10, 0.13, 0.09, and 0.06 mm min^{-1}, respectively. As the initial concentration of the metals increased, the rate-limiting step of adsorption gradually switched to intraparticle diffusion control, *i.e.*, the external diffusion model was not invalid with insignificant R^2 values.

Fig. 4 shows the fitting curves at different initial concentrations accompanied by the least-square regression analysis of the models. It was found that the intraparticle diffusion coefficient (k_p) increased significantly with the increase in the initial concentration of the metals. The best-fit lines for the intraparticle-diffusion model did not pass through the origin, indicating that there was an initial boundary layer resistance.

Table 2 Kinetic data extracted from various types of models for the adsorption of metal ions using time-lapse capsules at 20 °C

		Pseudo-first order			Pseudo-second order			
Metal	Concn.	k_1 (min^{-1})	k_1t_{ref} (−)	R^2	k_2 (g mg^{-1} min^{-1})	q_{max} (mg g^{-1})	R^2	$t_{1/2}$ (min)
Zn	C1	0.060 ± 0.002	3.612	0.987	3.205	0.037	0.995	8.4
	C2	0.044 ± 0.001	2.658	0.985	0.213	0.304	0.995	15.4
	C3	0.050 ± 0.004	2.988	0.923	0.042	2.200	0.999	10.8
	C4	0.041 ± 0.004	2.454	0.851	0.026	3.587	0.995	10.7
Pb	C1	0.080 ± 0.004	4.794	0.970	28.66	0.006	0.997	5.8
	C2	0.037 ± 0.001	2.238	0.994	0.525	0.064	0.885	29.8
	C3	0.067 ± 0.004	4.038	0.956	0.289	0.515	0.997	6.7
	C4	0.066 ± 0.003	3.930	0.970	0.089	1.151	0.993	9.8
Cu	C1	0.057 ± 0.002	3.408	0.984	3.513	0.020	0.992	14.2
	C2	0.034 ± 0.001	2.034	0.995	0.203	0.185	0.958	26.6
	C3	0.045 ± 0.004	2.676	0.888	0.054	1.643	0.997	11.3
	C4	0.078 ± 0.003	4.686	0.975	0.070	2.232	0.996	6.4
Cr	C1	0.059 ± 0.001	3.552	0.995	7.138	0.013	0.997	10.8
	C2	0.035 ± 0.001	2.088	0.980	0.486	0.118	0.992	17.4
	C3	0.073 ± 0.004	4.368	0.960	0.155	1.282	0.999	5.0
	C4	0.040 ± 0.001	2.412	0.985	0.030	2.139	0.980	15.6
Ni	C1	0.071 ± 0.003	4.284	0.982	22.42	0.007	0.995	6.4
	C2	0.038 ± 0.002	2.286	0.974	1.251	0.059	0.990	13.5
	C3	0.048 ± 0.004	2.874	0.878	0.200	0.538	0.996	9.3
	C4	0.041 ± 0.005	2.484	0.718	0.173	0.847	0.991	6.8
Ca	C1	0.062 ± 0.001	3.696	0.994	0.662	0.130	0.995	11.6
	C2	0.040 ± 0.002	2.400	0.963	0.073	1.241	0.990	11.0
	C3	0.053 ± 0.004	3.162	0.912	0.018	5.294	0.998	10.5
	C4	0.042 ± 0.002	2.502	0.975	0.006	10.02	0.989	16.6
Mn	C1	0.060 ± 0.001	3.588	0.995	6.543	0.013	0.995	11.8
	C2	0.037 ± 0.001	2.214	0.984	0.521	0.115	0.989	16.7
	C3	0.050 ± 0.004	3.012	0.889	0.112	0.987	0.999	9.0
	C4	0.052 ± 0.004	3.120	0.910	0.078	1.575	0.996	8.1
Ti	C1	0.061 ± 0.001	3.624	0.998	12.52	0.006	0.994	13.3
	C2	0.035 ± 0.001	2.094	0.985	0.902	0.056	0.993	19.8
	C3	0.077 ± 0.003	4.590	0.984	0.493	0.158	0.960	12.8
	C4	0.071 ± 0.011	4.254	0.602	2.691	0.117	0.999	3.2

Open Access Article. Published on 25 April 2020. Downloaded on 2/25/2026 9:47:25 AM.
This article is licensed under a Creative Commons Attribution-NonCommercial 3.0 Unported Licence.

Open Access Article. Published on 25 April 2020. Downloaded on 2/25/2026 9:47:25 AM.
This article is licensed under a Creative Commons Attribution-NonCommercial 3.0 Unported Licence.

Table 3 Kinetic data extracted from film-pore diffusion mechanism models for the adsorption of metal ions using time-lapse capsules at 20 °C

		External diffusion		Intraparticle diffusion			
Metal	Concn.	k_f (mm min^{-1})	R^2	$k_{p,1}$ (mg g^{-1} min$^{-1/2}$) × 10^3	R^2	$k_{p,2}$ (mg g^{-1} min$^{-1/2}$) × 10^3	R^2
Zn	C1	0.097 ± 0.007	0.933	5.2 ± 0.2	0.995	1.2 ± 0.6	0.779
	C2	0.096 ± 0.002	0.994	41.3 ± 1.2	0.996	10.5 ± 2.8	0.932
	C3	0.059 ± 0.007	0.763	354.4 ± 18.1	0.987	55.6 ± 6.8	0.985
	C4	0.021 ± 0.004	0.474	502.8 ± 53.0	0.947	111.4 ± 13.1	0.986
Pb	C1	0.083 ± 0.012	0.672	0.8 ± 0.0	0.990	0.2 ± 0.1	0.830
	C2	0.116 ± 0.006	0.969	7.1 ± 0.3	0.991	2.7 ± 0.6	0.955
	C3	0.086 ± 0.011	0.767	86.4 ± 5.2	0.983	7.6 ± 2.5	0.899
	C4	0.041 ± 0.006	0.672	151.8 ± 11.3	0.973	38.2 ± 2.4	0.716
Cu	C1	0.097 ± 0.005	0.957	2.5 ± 0.1	0.996	0.7 ± 0.5	0.660
	C2	0.107 ± 0.006	0.967	20.2 ± 1.6	0.968	9.3 ± 2.0	0.957
	C3	0.072 ± 0.006	0.891	258.1 ± 14.0	0.986	47.4 ± 0.9	0.999
	C4	0.021 ± 0.004	0.144	331.6 ± 44.5	0.917	29.2 ± 16.5	0.758
Cr	C1	0.140 ± 0.001	0.999	1.8 ± 0.1	0.985	0.3 ± 0.2	0.660
	C2	0.092 ± 0.003	0.988	14.1 ± 0.4	0.997	5.9 ± 1.1	0.966
	C3	0.122 ± 0.009	0.905	199.6 ± 19.1	0.956	18.2 ± 8.3	0.826
	C4	0.062 ± 0.004	0.955	230.0 ± 5.9	0.997	121.2 ± 51.9	0.845
Ni	C1	0.052 ± 0.003	0.939	0.8 ± 0.0	0.990	0.2 ± 0.1	0.660
	C2	0.097 ± 0.003	0.990	7.4 ± 0.2	0.994	2.9 ± 0.5	0.971
	C3	0.074 ± 0.007	0.860	85.2 ± 4.2	0.988	13.4 ± 0.5	0.999
	C4	0.025 ± 0.004	0.314	107.3 ± 12.4	0.937	24.3 ± 7.4	0.915
Ca	C1	0.168 ± 0.017	0.876	19.7 ± 0.6	0.995	3.5 ± 0.0	1.000
	C2	0.127 ± 0.007	0.963	153.9 ± 4.0	0.997	55.0 ± 12.4	0.952
	C3	0.081 ± 0.007	0.862	883.4 ± 54.8	0.981	116.1 ± 12.9	0.988
	C4	0.031 ± 0.004	0.734	1246 ± 107	0.964	387.2 ± 99.8	0.938
Mn	C1	0.107 ± 0.005	0.965	1.9 ± 0.1	0.982	0.3 ± 0.2	0.660
	C2	0.093 ± 0.002	0.993	14.0 ± 0.6	0.992	5.6 ± 1.1	0.964
	C3	0.067 ± 0.008	0.787	160.3 ± 9.3	0.983	23.8 ± 1.4	0.997
	C4	0.023 ± 0.004	0.359	225.1 ± 29.1	0.923	34.9 ± 5.1	0.979
Ti	C1	0.078 ± 0.007	0.874	0.8 ± 0.0	0.990	0.2 ± 0.1	0.660
	C2	0.063 ± 0.002	0.979	6.7 ± 0.4	0.990	2.7 ± 0.6	0.955
	C3	0.025 ± 0.005	0.324	27.5 ± 1.9	0.978	1.7 ± 1.0	0.743
	C4	0.006 ± 0.002	0.532	20.0 ± 3.5	0.868	0.9 ± 0.2	0.946

For the intraparticle-diffusion model, the boundary layer effect became more significant as the intercept of the fitting curves increased. As shown in Fig. 4(e–h), a multilinearity for intraparticle-diffusion models was observed, indicating that multiple steps of mechanism occurred during the adsorption process: the rapid diffusion (phase I) and the slow diffusion

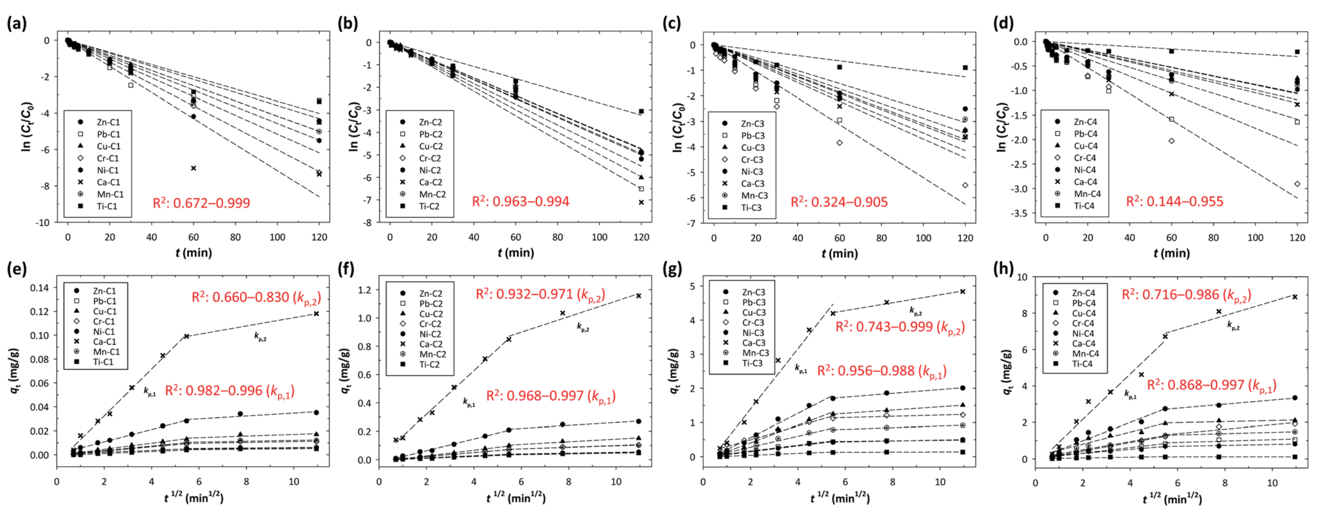

Fig. 4 External diffusion model curves for specific rate constant of metal ions on time-lapse capsules at different initial concentrations: (a) C1, (b) C2, (c) C3, and (d) C4. Intraparticle diffusion model at different initial concentrations: (e) C1, (f) C2, (g) C3, and (h) C4, where the regression curves consist of two linear segments with different slopes.

Open Access Article. Published on 25 April 2020. Downloaded on 2/25/2026 9:47:25 AM.
This article is licensed under a Creative Commons Attribution-NonCommercial 3.0 Unported Licence.

(phase II). In phase I (the first linear segment, corresponding to $k_{p,1}$), macro-pore diffusion was dominant with instantaneous occupation of the available adsorbing sites on the surface of the resins. In contrast, in phase II (the second linear segment, corresponding to $k_{p,2}$), micro-pore diffusion was dominant with slow diffusion of metals from the surface film into the micro-pores, as well as slow migration of metals from the liquid phase onto the surface of the resins.

3.3 Adsorption equilibrium and isotherm

Adsorption isotherms are essential for the design of adsorption systems as they describe the relationship between the equilibrium concentration of metal ions in the solution (C_e) and the amount of metal ions adsorbed onto the adsorbent (q_e) at a constant temperature. The data from adsorption isotherm models can provide information about the adsorption capacity of the adsorbent, as well as the prediction of adsorption parameters. Table 4 presents the adsorption isotherm parameters for different metal ions using time-lapse capsules at 20 °C. The results indicated that three isotherm models, *viz.*, the Langmuir, Temkin, and D–R models, fitted very well for most of the metal ions. The coefficients of determination for the Langmuir, Temkin, and D–R models were in the range of 0.973–1.000 (except for Ti), 0.824–0.987 (except for Cr), and 0.811–0.995 (except for Pb), respectively.

From the Langmuir model, the maximum adsorption capacities (q_m) for Zn, Pb, Cu, Cr, Ni, Ca, and Mn were found to be 2.8, 2.7, 6.3, 16.3, 6.4, 10.9, and 4.2 mg g^{-1}, respectively. The adsorption energy constants (K_L) for Zn, Pb, Cu, Cr, Ni, Ca, and Mn were 1.24, 0.42, 0.34, 0.12, 0.13, 0.83, and 0.36 L mg^{-1}, respectively. To describe the affinity between the adsorbents and the metal ions, the concept of separation factor (R_L, dimensionless) was applied as determined by eqn (23):

$$R_L = \frac{1}{1 + K_L C_0} \tag{23}$$

where C_0 is the initial concentration of metal ions in the solution (mg L^{-1}). When $0 < R_L < 1$, the adsorption process is favorable; when the $R_L = 1$, the adsorption process is linear; when $R_L = 0$, the process is irreversible; when $R_L > 1$, the adsorption process is unfavorable.[28] In this study, the R_L values for all the metal ions (except for Ti) ranged between 0 and 1, indicating the favorable adsorption of the metal ions using the time-lapse capsules. The adsorption isotherm had a convex shape, representing enhanced adsorption at low concentrations.[23]

The Temkin model could also well predict the adsorption behavior of most of the metal ions, except for Cr and Ti. The obtained K_T values for Zn, Pb, Cu, Ni, Ca, and Mn were 0.08, 0.44, 0.30, 0.92, 0.38, and 0.51 L mg^{-1}, respectively. The equilibrium binding constant was related to the maximum binding energy. The heat of adsorption (b) for Zn, Pb, Cu, Ni, Ca, and Mn was 6.3, 19.3, 10.4, 27.9, 3.0, and 15.0 J mol^{-1}, respectively.

The adsorption of Ti could be well described only by the D–R model, with a high R^2 value of 0.995. The D–R model could also be used to predict the adsorption of most of the metal ions, except for Pb and Cr. The determined E values for Zn, Cu, Ni, Ca, Mn, and Ti were 27.5, 29.4, 32.4, 31.5, 30.5, and 31.1 kJ mol^{-1}, respectively. E values higher than 8 kJ mol^{-1} indicated chemisorption,[29] which would follow the ion-exchange mechanism. The obtained results from the isotherm models were consistent with that from the kinetic models. The obtained q_m values for Zn, Cu, Ni, Ca, Mn, and Ti were 0.002, 0.002, 0.001, 0.001, 0.006, and 0.001 mg g^{-1}, respectively.

3.4 Insights into the fundamentals and practical applications

In this study, three different approaches, *i.e.*, response surfaces (from the statistical point of view, see Table 1), time-related and/or diffusion-controlled models (from the kinetic point of view, see Table 2), and adsorption isotherm (from the equilibrium point of view, see Table 3), were utilized to evaluate the effect of operating factors on the entrapment of heavy metals from water using time-lapse capsules. The response surface models were established based on the experimental design to describe the adsorption behaviors of different metal ions with respect to various operating parameters. Since they were developed from the statistical point of view, the obtained coefficients usually have no physical meanings. However, based on these empirical response surfaces, one could easily identify the operating conditions for achieving the maximum adsorption ratio. One

Table 4 Adsorption isotherm parameters for different metal ions using time-lapse capsules at 20 °C

	(1) Langmuir				(2) Freundlich			(3) Temkin			(4) Dubinin–Radushkevich		
Metals	K_L (L mg^{-1})	q_m (mg g^{-1})	R^2	R_L [a]	K_F	n (−)	R^2	K_T (L mg^{-1})	b (kJ mol^{-1})	R^2	q_m (mg g^{-1})	E (kJ mol^{-1})	R^2
Zn	1.24	2.75	0.998	0.13	0.70	2.01	0.872	0.08	6.3	0.975	0.0024	27.5	0.977
Pb	0.42	2.71	0.973	0.70	0.53	1.84	0.617	0.44	19.3	0.921	0.0006	31.8	0.464
Cu	0.34	6.30	1.000	0.50	0.66	2.15	0.738	0.30	10.4	0.987	0.0020	29.4	0.919
Cr	0.12	16.3	0.985	0.79	1.82	1.75	0.891	1.87	11.7	0.722	0.0011	34.2	0.811
Ni	0.13	6.37	1.000	0.88	0.44	2.02	0.892	0.92	27.9	0.949	0.0006	32.4	0.981
Ca	0.83	10.9	0.999	0.05	2.56	2.64	0.854	0.38	3.0	0.951	0.0063	31.5	0.971
Mn	0.36	4.23	0.999	0.58	0.52	1.98	0.895	0.31	15.0	0.957	0.0011	30.5	0.971
Ti	— [b]	— [b]	— [b]	— [b]	0.08	2.56	0.749	0.50	152.3	0.824	0.0001	31.1	0.995

[a] R_L values were determined at the concentration in accordance with Taiwan EPA's effluent standards (*i.e.*, C2). [b] The obtained values were meaningless.

 This journal is © The Royal Society of Chemistry 2020

Open Access Article. Published on 25 April 2020. Downloaded on 2/25/2026 9:47:25 AM. This article is licensed under a Creative Commons Attribution-NonCommercial 3.0 Unported Licence.

way to enhance the fundamental basis (physically meaningful) of the response surface models was to combine it with the unit-factor method, *i.e.*, using dimensionless groups as the equation inputs. The concept of dimensional homogeneity could be utilized in the design of process scale-up.

Conversely, the kinetic models (such as diffusion-controlled kinetics) were applied to determine the rate-limiting step in a heterogeneous system based on the fundamental mechanisms and theories. These classical kinetic models have been widely used because of their conceptual and mathematical simplicity, compared to the models based on numerical analysis. The key design parameters of the time-lapse capsules, for *e.g.*, the adsorption rate constant and diffusion coefficient, could be obtained with these kinetic models. The obtained constants and/or coefficients could provide information about the adsorption behaviors at the liquid–solid interface. Hence, it was assumed that these models could be applied for future scale-up and optimization. Likewise, the adsorption isotherm models were developed based on the fundamentals of equilibrium adsorption with respect to different initial concentrations at a constant temperature. The obtained isotherm data described the equilibrium relationship between the time-lapse capsules (adsorbent) and the heavy metals (adsorbate). The distributions of different heavy metals between the time-lapse capsules and the water solution at equilibrium were useful for estimating the maximum adsorption capacity of the designed systems.

This research should be considered as the pioneering study reporting the adsorption kinetics and capacities of different heavy metals using time-lapse capsules, which could be used as the design criteria for future improvement. The concept of developing low-cost materials (*i.e.*, time-lapse capsules) provides an insight into the *in situ* and simple monitoring of heavy metals in water bodies. In practice, the deployment of time-lapse capsules can easily identify the potential sources and patterns of illegal or accidental discharges containing heavy metals from industries into natural water bodies without intensive labor. In addition, the time-lapse capsules can be possibly used to capture trace emerging contaminants, such as perfluorooctanoic and perfluorooctanesulfonic acids, from an aqueous environment by concentrating them onto the ion-exchange resins over a period of time. This technique exhibits a great potential of wide applications in tracking or extracting various types of pollutants (even at the sub-ppm level) from water bodies and/or paddy soils at low cost. In our previous study,[30] we successfully utilized the XRF technique to rapidly determine the concentrations of heavy metals adsorbed on the time-lapse capsules. For the sake of heavy metal monitoring, the regeneration of the used ion-exchange resins was not necessary as the time-lapse capsules were designed for one-time use.

3.5 Priority research directions: adsorption behaviors and interactions

In this study, we have provided an insight into the adsorption behaviors of different heavy metals using time-lapse capsules from different angles by using a multiple model approach. The obtained kinetic and isotherm parameters could be used to improve the design of time-lapse capsules. In this section, we have proposed several priority research directions for future studies, including (1) sorption kinetics adapted to field operations, (2) interactions and competitive sorption of different heavy metals, and (3) contribution of electrostatic sorption and complexation.

3.5.1 Sorption kinetics adapted to field operations. In this study, we conducted batch adsorption experiments in a controlled environment, such as fixed temperature and pH. However, in the real case of field operations, these operating factors would be variable. Therefore, the effect of the operating factors that are particularly related to the real water body, such as pH, temperature, mixing, and dosage of resins, on the adsorption kinetics and capacity should be further evaluated. It is noted that these factors generally play significant roles in the adsorption kinetics and thus, influence the maximum adsorption capacity. For instance, different adsorption behaviors of heavy metals at different pH values could be observed due to the different ionic forms of heavy metals present in the real water body at different pH values. For different temperatures, key thermodynamic parameters such as Gibbs free energy of adsorption could be determined accordingly. For the mixing, experiments at different stirring speeds conducted in the laboratory should be further correlated with the Reynold (Re) number to predict the performance of adsorption in the real water body.

3.5.2 Interactions and competitive sorption of different heavy metals. Real water bodies are multi-component systems where various types of inorganic and organic compounds exist. The presence of multiple solutes could significantly affect the adsorption rates and capacities of the ion-exchange resins for different metals. In other words, the interactions and competitive uptake of different heavy metals from the real river samples using the time-lapse capsules should be evaluated to understand the simultaneous adsorption behaviors and interactions involving more metal ions. A set of competitive sorption models for multi-component systems, such as the extended/modified Langmuir equation,[31] the IAST-based Sips equation,[32] the Sheindorf–Rebhun–Sheintuch model,[33] and the modified Redlich–Peterson equation,[34] could be applied to evaluate the adsorption behavior and isotherms.

3.5.3 Contribution of electrostatic sorption and complexation. The understanding of adsorption mechanism pathways with proper interpretation of adsorption isotherms is crucial for the effective improvement of adsorption system design. From the fundamental point of view, the possible mechanisms of adsorption include physisorption, chemisorption, electrostatic sorption, complex formation, and hydrate formation.[10] To understand the contributions of different mechanisms to the interactions between the ion-exchange resins and heavy metals, an integrated mechanistic model considering electrostatic sorption, complex formation, and hydrate formation shall be developed in our future work. Pehlivan *et al.*[35] suggested that, along with chemisorption, the contribution of electrostatic sorption and complexation are important. For hydrate formation, the radius and dehydration degree of the adsorbed

Open Access Article. Published on 25 April 2020. Downloaded on 2/25/2026 9:47:25 AM. This article is licensed under a Creative Commons Attribution-NonCommercial 3.0 Unported Licence.

metallic species should be determined and integrated into the mechanistic model.

4. Conclusion

In this study, multiple model approaches including response surfaces, kinetics, and isotherms were utilized to evaluate the effect of operating factors on the performance of trapping heavy metals from water using time-lapse capsules. The results indicated that the adsorption of metal ions on the time-lapse capsules proceeded in two stages in the period of contact time, *viz.*, (i) rapid uptake, especially within the beginning 20 min and (ii) slow adsorption after 40 min. This could be attributed to the available active sites on the ion-exchange resins. According to the kinetic analyses, it was suggested that adsorption was due to chemisorption and the adsorption mechanism was adsorbate diffusion rather than surface control. The rate-limiting step would be external diffusion control at low initial concentrations, which gradually switched to intraparticle diffusion control as the initial concentration of metals increased. The results from the intraparticle-diffusion models also indicated that there was an initial boundary layer resistance. The obtained external diffusion coefficients for Zn, Pb, Cu, Cr, Ni, Ca, Mn, and Ti were 0.10, 0.12, 0.11, 0.09, 0.10, 0.13, 0.09, and 0.06 mm min^{-1}, respectively. Similarly, the results of the isotherm models indicated favorable adsorption of the metal ions using time-lapse capsules. Both the Langmuir and Temkin isotherm models fitted well for the adsorption behavior of most of the metal ions, while the adsorption of Ti could be well described only by the D–R isotherm model. In order to enhance the fundamental knowledge of heavy metal adsorption using time-lapse capsules, our future work will be focused on the contribution of electrostatic adsorption and complexation to adsorption, as well as the competitive adsorption of different heavy metals.

Conflicts of interest

There are no conflicts to declare.

Acknowledgements

High appreciation goes to the Council of Agriculture, Executive Yuan, Taiwan (ROC) for the financial support under Grant number 106AS-15.2.2-IE-b1 and 1082101021901-110201b1. Shu-Yuan Pan also thanks the financial support from National Taiwan University under the Grant Number 109L7303 and from Ministry of Science and Technology (MOST) under the Grant Number 108-2636-M-002-012.

References

1 Y. Owusu-Asante, Analysis and determination of optimum risk factors to prioritize illegal discharge potential in urban catchments, *Phys. Chem. Earth*, 2019, **111**, 86–99.

2 F. Xia, L. Qu, T. Wang, L. Luo, H. Chen, R. A. Dahlgren, M. Zhang, K. Mei and H. Huang, Distribution and source analysis of heavy metal pollutants in sediments of a rapid developing urban river system, *Chemosphere*, 2018, **207**, 218–228.

3 J. S. Huang, S. C. Lin, L. Lowemark, S. Y. H. Liou, Q. Chang, T. K. Chang, K. Y. Wei and I. W. Croudace, Rapid assessment of heavy metal pollution using ion-exchange resin sachets and micro-XRF core-scanning, *Sci. Rep.*, 2019, **9**, 6601.

4 F.-Q. An, Y. Wang, X.-Y. Xue, T.-P. Hu, J.-F. Gao and B.-J. Gao, Design and application of thiourea modified D301 resin for the effective removal of toxic heavy metal ions, *Chem. Eng. Res. Des.*, 2018, **130**, 78–86.

5 K. Xiao, F. Xu, L. Jiang, Z. Dan and N. Duan, The oxidative degradation of polystyrene resins on the removal of Cr(VI) from wastewater by anion exchange, *Chemosphere*, 2016, **156**, 326–333.

6 F. Dixit, B. Barbeau, S. G. Mostafavi and M. Mohseni, PFOA and PFOS removal by ion exchange for water reuse and drinking applications: role of organic matter characteristics, *Environ. Sci.: Water Res. Technol.*, 2019, **5**, 1782–1795.

7 G. Bayramoglu, A. Akbulut, G. Liman and M. Y. Arica, Removal of metal complexed azo dyes from aqueous solution using tris(2-aminoethyl)amine ligand modified magnetic p(GMA-EGDMA) cationic resin: Adsorption, isotherm and kinetic studies, *Chem. Eng. Res. Des.*, 2017, **124**, 85–97.

8 W. A. Tarpeh, I. Wald, M. Wiprächtiger and K. L. Nelson, Effects of operating and design parameters on ion exchange columns for nutrient recovery from urine, *Environ. Sci.: Water Res. Technol.*, 2018, **4**, 828–838.

9 S. Gámez, K. Garcés, E. de la Torre and A. Guevara, Precious metals recovery from waste printed circuit boards using thiosulfate leaching and ion exchange resin, *Hydrometallurgy*, 2019, **186**, 1–11.

10 R. K. Nekouei, F. Pahlevani, M. Assefi, S. Maroufi and V. Sahajwalla, Selective isolation of heavy metals from spent electronic waste solution by macroporous ion-exchange resins, *J. Hazard. Mater.*, 2019, **371**, 389–396.

11 P.-K. Shih, L.-C. Chiang, S.-C. Lin, T.-K. Chang and W.-C. Hsu, Application of Time-Lapse Ion Exchange Resin Sachets (TIERS) for Detecting Illegal Effluent Discharge in Mixed Industrial and Agricultural Areas, *Sustainability*, 2019, **11**, 3129.

12 J. Ma, J. Shen, C. Wang and Y. Wei, Preparation of dual-function chelating resin with high capacity and adjustable adsorption selectivity to variety of heavy metal ions, *J. Taiwan Inst. Chem. Eng.*, 2018, **91**, 532–538.

13 B. J. Ni, Q. S. Huang, C. Wang, T. Y. Ni, J. Sun and W. Wei, Competitive adsorption of heavy metals in aqueous solution onto biochar derived from anaerobically digested sludge, *Chemosphere*, 2019, **219**, 351–357.

14 EPA Taiwan, Database: Clearance of Municipal Solid Waste by Implementing Agencies, 2018, Data Period: 1998/01/01 to 2018/05/31.

15 S. Lagergren, About the theory of so-called adsorption of soluble substances, *K. Sven. Vetenskapsakad. Handl.*, 1898, **24**, 1–39.

This journal is © The Royal Society of Chemistry 2020

Open Access Article. Published on 25 April 2020. Downloaded on 2/25/2026 9:47:25 AM. This article is licensed under a Creative Commons Attribution-NonCommercial 3.0 Unported Licence.

16 Y. S. Ho and G. McKay, Pseudo-second order model for sorption processes, *Process Biochem.*, 1999, **34**, 451–465.
17 E.-A. Kwak, S.-J. Kim and J.-H. Kim, Effect of ion exchange resin on increased surface area crystallization process for purification of vancomycin, *Korean J. Chem. Eng.*, 2012, **29**, 1487–1492.
18 W. J. Weber and J. C. Morris, presented in part at the *Proceedings of International Conference on Water Pollution Symposium*, 1962.
19 S. S. Dubey and R. K. Gupta, Removal behavior of Babool bark (Acacia nilotica) for submicro concentrations of Hg^{2+} from aqueous solutions: a radiotracer study, *Sep. Purif. Technol.*, 2005, **41**, 21–28.
20 A. S. Özcan, B. Erdem and A. Özcan, Adsorption of Acid Blue 193 from aqueous solutions onto BTMA-bentonite, *Colloids Surf., A*, 2005, **266**, 73–81.
21 M. H. El-Naas, S. Al-Zuhair and M. A. Alhaija, Removal of phenol from petroleum refinery wastewater through adsorption on date-pit activated carbon, *Chem. Eng. J.*, 2010, **162**, 997–1005.
22 M. S. Onyango, Y. Kojima, O. Aoyi, E. C. Bernardo and H. Matsuda, Adsorption equilibrium modeling and solution chemistry dependence of fluoride removal from water by trivalent-cation-exchanged zeolite F-9, *J. Colloid Interface Sci.*, 2004, **279**, 341–350.
23 A. Gabelman, *Adsorption Basics: Part 1*, American Institute of Chemical Engineering, 2017, pp. 48–53.
24 L. Li, F. Liu, X. Jing, P. Ling and A. Li, Displacement mechanism of binary competitive adsorption for aqueous divalent metal ions onto a novel IDA-chelating resin: isotherm and kinetic modeling, *Water Res.*, 2011, **45**, 1177–1188.
25 M. Assefi, S. Maroufi, R. K. Nekouei and V. Sahajwalla, Selective recovery of indium from scrap LCD panels using macroporous resins, *J. Cleaner Prod.*, 2018, **180**, 814–822.
26 Y. N. Thakare and A. K. Jana, Performance of high density ion exchange resin (INDION225H) for removal of Cu(II) from waste water, *J. Environ. Chem. Eng.*, 2015, **3**, 1393–1398.
27 M. Doğan, Y. Özdemir and M. Alkan, Adsorption kinetics and mechanism of cationic methyl violet and methylene blue dyes onto sepiolite, *Dyes Pigm.*, 2007, **75**, 701–713.
28 M. M. Rao, A. Ramesh, G. P. C. Rao and K. Seshaiah, Removal of copper and cadmium from the aqueous solutions by activated carbon derived from Ceiba pentandra hulls, *J. Hazard. Mater.*, 2006, **129**, 123–129.
29 F.-Q. An, R.-Y. Wu, M. Li, T.-P. Hu, J.-F. Gao and Z.-G. Yuan, Adsorption of heavy metal ions by iminodiacetic acid functionalized D301 resin: Kinetics, isotherms and thermodynamics, *React. Funct. Polym.*, 2017, **118**, 42–50.
30 W. J. Syu, T. K. Chang and S. Y. Pan, Establishment of an Automatic Real-Time Monitoring System for Irrigation Water Quality Management, *Int. J. Environ. Res. Public Health*, 2020, **17**(3), 737.
31 X.-P. Zhang, F.-Q. Liu, C.-Q. Zhu, C. Xu, D. Chen, M.-M. Wei, J. Liu, C.-H. Li, C. Ling, A.-M. Li and X.-Z. You, A novel tetraethylenepentamine functionalized polymeric adsorbent for enhanced removal and selective recovery of heavy metal ions from saline solutions, *RSC Adv.*, 2015, **5**, 75985–75997.
32 S. Khalili, B. Khoshandam and M. Jahanshahi, Synthesis of activated carbon/polyaniline nanocomposites for enhanced CO_2 adsorption, *RSC Adv.*, 2016, **6**, 35692–35704.
33 Z. Wu, Z. Sun, P. Liu, Q. Li, R. Yang and X. Yang, Competitive adsorption of naphthalene and phenanthrene on walnut shell based activated carbon and the verification via theoretical calculation, *RSC Adv.*, 2020, **10**, 10703–10714.
34 O. Kazak, A. Tor, I. Akin and G. Arslan, Preparation and characterization of novel polysulfone-red mud composite capsules for the removal of fluoride from aqueous solutions, *RSC Adv.*, 2016, **6**, 86673–86681.
35 E. Pehlivan and T. Altun, Ion-exchange of Pb^{2+}, Cu^{2+}, Zn^{2+}, Cd^{2+}, and Ni^{2+} ions from aqueous solution by Lewatit CNP 80, *J. Hazard. Mater.*, 2007, **140**, 299–307.